International Journal of Nanoelectronics and Materials
Volume 16 (Special Issue) December 2023 [169-182]

Synthesis and Characterization of $SrTiO_3$ Doped with $Bi(CH_3COO)_3$

Mahfuddin Zuhri*, Hilal Fauzi Ramadhan, Irzaman

Department of Physics, Faculty of Mathematics and Natural Sciences, IPB University, Bogor 16680, Indonesia

ABSTRACT

Synthesis of Strontium Titanate ($SrTiO_3$) doped with Bismuth Acetatem ($Bi(CH_3COO)_3$) has been successfully carried out with varying concentrations of 0%; 0.5%; 1%; and 1.5% impurity in weight percent. The concentrated solution was dripped onto a P- type silicon substrate (1 0 0) using the Chemical Solution Deposition (CSD) method and spin coating technique. Annealing process was carried out with a temperature increase of 1.67oC/minute and held at 850oC for 8 hours and then cooled to room temperature for 12 hours. The film thickness was determined by the volumetric method, resulting in values of 3.9 µm, 4.3 µm, 4.7 µm and 5.1 µm. The analysis of optical properties with the Kubelka-Munk function for the direct transition results a band gap of 3.46 - 3.56 eV. Analysis of the XRD results was carried out using the Cramer-Cohen method and obtained lattice parameters (a=b=c) of Strontium Titanate ($SrTiO_3$) doped with Bismuth Acetate ($Bi(CH_3COO)_3$) with various concentrations of 0%; 0.5%; 1%; and 1.5% are 3.835 Å, 3.837 Å, 3.909 Å, 3.913 Å respectively with a cubic crystal structure. This is because the ionic radius of bismuth (1.32 Å) is larger than that of strontium (1.17 Å), so bismuth will replace strontium in thin films. This replacement causes the lattice parameter values to increase, and effects the XRD spectral curve at the preferred peak (1 1 0) shift to the left. This shows that the doping bismuth has entered the strontium host.

Keywords: CSD, energy band gap, lattice parameter, spin coating, $SrTiO_3$

1. INTRODUCTION

The development of electronic material technology has progressed very rapidly, one of which is ferroelectric material. The advantage of ferroelectric materials is the ability to change the internal polarization using a suitable electric field and spontaneous polarization. Ferroelectric materials have several unique properties, including hysteresis properties and high dielectric constant, piezoelectric properties, pyroelectric properties, and linear optical properties for thin films [1]. Thin films made from ferroelectric materials can be used as switches, light detectors, and automatic devices that use optical principles in their work systems [2].

Strontium Titanate ($SrTiO_3$) is a ferroelectric material that is widely used in the form of thin films. $SrTiO_3$ is a metal oxide material that has a cubic perovskite structure with physical properties such as paraelectricity, superconductivity and photocatalysis. The advantages of $SrTiO_3$ lie in its good chemical properties and physical stability, as well as superior optical properties [3]. Based on these properties, several applications can be developed including capacitors, microwave devices, and photocatalysts [4].

The perovskite structure is a crystal structure that has the general formula ABX3, with A and B representing different-sized cations where A is Sr from the alkaline earth group and B is Ti from the transition group. Whereas X (Anion) is a halogen group such as O, Cl, Br, or I [5,6]. The crystal structure of $SrTiO_3$ is shown in Figure 1. $SrTiO_3$ has the unit formula perovskite cubic ABO_3 where A and B are metal cations and O is an oxygen anion [7]. $SrTiO_3$ has an indirect band gap of 3.25 eV

* Corresponding authors: mahfuddinzh@apps.ipb.ac.id

and a direct band gap of 3.75 eV [8]. At room temperature, the perovskite structure has a cubic unit cell and a lattice parameter length of 3.905 Å.

The strength of the conducting properties of SrTiO3 depends on the number of negative or positive charge carriers. If the carrier is negatively charged (electrons) then SrTiO3 is called an n-type semiconductor, conversely, if the carrier is positively charged (holes/holes) then SrTiO3 is a p-type semiconductor [5].

$SrTiO_3$ is a mixture of reaction products between Strontium Acetate $Sr(CH_3COO)_2$ and Titanium Isopropoxide $Ti(C_{12}H_{28}O_4)$. The following is the reaction equation in the manufacture of strontium titanate equation (1):

$$Sr(CH_3COO)_2 + Ti(C_{12}H_{28}O_4) + O_2 \rightarrow SrTiO_3 + CO_2 + H_2O \quad (1)$$

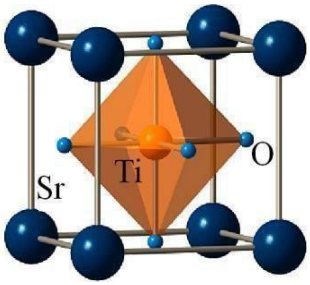

Figure 1. $SrTiO_3$ crystal structure [5].

The performance and properties of a semiconductor material can be improved by adding impurities, one of which is Bismuth. Bismuth is the 83rd element in the periodic table of elements that has been known for a long time [9]. Bismuth is a material of great interest because of its small effective electron mass, high electron value, and highly anisotropic Fermi surface. The electrical properties of Bismuth are closely related to its microstructure and are compatible with the process of deposition or growth of thin films [10]. Bismuth is identified as a semimetal that has semiconducting properties whose resistivity depends on temperature and the concentration of charge carriers is lower than that of metals [11]. The bismuth used in this study was Bismuth (III) Acetate as a thin film impurity. Bismuth (III) Acetate is an inorganic compound consisting of positive bismuth ions (charge 3+) and negative ions (charge 1-). Bismuth (III) Acetate is usually used as a precursor for synthesis with other materials so that it can be applied in the field of physics [12]. The advantages of Bismuth (III) Acetate include having a high molecular weight, fairly good stoichiometry, relatively cheap price, and low toxicity.

2. MATERIAL AND METHOD

The research procedures included substrate preparation, solution preparation, $SrTiO_3$ film growth, annealing stage, and characterization.

2.1 Substrate Preparation

The substrate used was p-type silicon (1 0 0) substrate. The substrate was cut with a size of 1 cm x 1 cm in 20 square pieces using a diamond blade knife. The 20 pieces of Si substrate (1 0 0) for 4 treatments and 5 replications. The substrate that has been cut is then cleaned by dipping the substrate into a measuring cup containing aquabides for 1 minute. The clean substrate is dried using a tissue slowly until dry. After that, measure the mass of the substrate using a digital balance, by weighing 3 times for each piece of substrate.

2.2 Solution Making

The process of making the solution in the first stage by preparing the chemicals to be used such as p- type (1 0 0) silicon (Si) substrate, Strontium Acetate powder, Titanium Isopropoxide solution, 2- methoxyethanol solvent, and Bismuth Acetate powder. The chemicals used were weighed first using a digital balance according to stoichiometric calculations at a solubility of 1 M. The strontium acetate powder that had been weighed was then put into a vial and added 10 drops of 2-methoxyethanol using a micropipette.

Then the vials were placed on a magnetic stirrer and stirred at 240 rpm for 30 minutes. Then drip titanium isoproxide slowly and rotated again for 30 minutes. For samples with impurities, Bismuth Acetate is mixed with strontium acetate with each reaction according to variations in impurities and rotated again for 30 minutes. This process yields a homogeneous solution. Table 1 shows composition of materials for making $SrTiO_3$ solution at 1 M solubility.

Table 1 Composition of materials for making SrTiO3 solution at 1 M solubility

Impurity variation (%)	Strontium (II) Acetate (g)	Titanium Isopropoxide (g)	Bismuth (III) Acetate (g)	2-Methoxyethanol (ml)
0	0.4114	0.5684	0	2
0.5	0.4094	0.5684	0.0039	2
1	0.4073	0.5684	0.0077	2
1.5	0.4052	0.5684	0.0116	2

2.3 $SrTiO_3$ Film Growth

The growth of $SrTiO_3$ thin films was carried out using the Chemical Solution Deposition (CSD) method and the spin coating technique. The inactive part of the silicon substrate surface is attached to the spin coating using double tape. The purpose of the substrate being attached is so that the substrate does not come off when the spin disc rotates. Half of the surface of the active substrate is covered using a tape and the other half is dripped with a homogeneous solution. The purpose of partially covering the substrate is to obtain p-type and n-type semiconductors. N-type semiconductor from Strontium Titanate solution and p-type from silicon substrate. The spin coating time is 60 seconds for three rounds with drops of 200 microliters and the spin setting is 8000 rpm [13].

2.4 Annealing Stage

The annealing stage is a heating process at room temperature, followed by a cooling process. This annealing process is carried out in the Nabertherm furnace. This stage can affect the strength of the layer or the ability of a layer to deform when given pressure. The intensity of each crystal field can change if the heating temperature also changes [14]. The annealing process has the goal of diffusing the solution on the substrate with high-temperature treatment. Different temperatures will result in different characterizations of thin films in terms of crystal structure, thickness, and grain size. In addition, the annealing process is intended so that the $SrTiO_3$ material and $Bi(CH_3COO)_3$ impurities can be firmly attached to the silicon substrate. The annealing process was carried out in stages, starting at room temperature and then increasing it to 850°C with an increase of 1.67oC/minute. The increase in room temperature to 850°C takes 8 hours and 20 minutes, then it is held for 15 hours and then the temperature drops from 850°C until it returns to room temperature. Then manual furnace cooling is carried out until it returns to room temperature [15]. The annealing process can be shown as shown in Figure 2 [16].

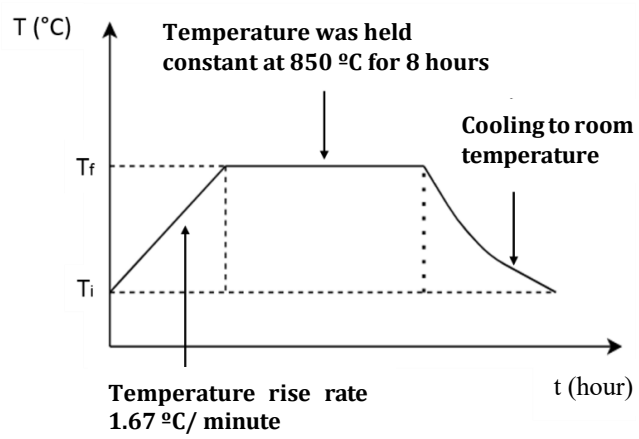

Figure 2. Annealing Process [16].

2.5 Annealing Stage

The thin film thickness was calculated after the annealing process was complete using the volumetric method. This method is carried out by first weighing the substrate that has not been coated with a thin film (m1) and reweighing the substrate that has been coated with a thin film (m2) [17] and repeated 4 times for each sample. Thin film thickness is calculated using the volumetric method with the equation (2):

$$d = \frac{m_2 - m_1}{\rho_{thin\ film} A} \tag{2}$$

which is
d = film thickness (cm)
m1 = mass of substrate before thin film growth (g)
m2 = mass of substrate after annealing and there is a thin film on it (g)
A = surface area of the thin film deposited on the surface of the substrate (cm^2)
$\rho_{thin\ film}$ = density of deposited thin film (g/cm^3)

2.6 Analysis of UV-Vis Spectrophotometer Results

The method used to analyze the UV-Vis spectrophotometer is the Kubelka-Munk method. The Kubelka-Munk method shows the relationship between reflectance, absorbance, and the scattering of light that occurs. This method is used to identify the sensitivity of the light spectrum of thin films so that the band gap energy can be estimated. It is also considered more effective for increasing the linearity of the spectrum, especially for measuring samples with small particles that link the reflection of the sample spectrum including the absorbance coefficient (K), Scattering coefficient (S), and Reflectance (R) as in the equation (3), (4), and (5):

$$F\ (R) = \frac{K}{S} = \frac{(1-R)^2}{2R} \propto \alpha_{K-M} \tag{3}$$

$$F\ (R) \propto \alpha_{K-M} \propto \frac{(hv - E_g)^{\frac{1}{n}}}{hv} \tag{4}$$

$$(\alpha_{K-M} hv)^n = A(hv - E_g) \tag{5}$$

2.7 Analysis of X-Ray Diffraction (XRD) Results

Data generated from XRD will be processed using the Cramer-Cohen method and MAUD software. MAUD software can be used to analyze material behavior using XRD diffraction pattern information. The output of the MAUD software is used to estimate the crystal size of the sample and is believed to be more precise when compared to using the Scherer equation and the Rietica software. MAUD software can also perform refinements in the form of changing parameters to match calculated and measured diffraction patterns [18].

3. RESULT AND DISCUSSION

3.1 $SrTiO_3$ Film Thickness

The concentration of impurities in the $SrTiO_3$ film was varied to determine the effect on the thickness of the thin film. 4 variations of impurity concentration were carried out, respectively 0%, 0.5%, 1%, and 1.5%. The thickness of $SrTiO_3$ was calculated using the volumetric method by applying equation (1). The calculation results are presented in Table 2.

Table 2 Film thickness based on variations in impurity concentration

Impurity (%)	m_1 (gram)	m_2 (gram)	Δm (gram)	ρ_{Film} (gram/cm^3)	Surface area (cm^2)	Film Thickness (μm)
0	0.126	0.127	0.001	5.122	0.5	3.9047
0.5	0.121	0.122	0.0011	5.122	0.5	4.2952
1	0.121	0.122	0.0012	5.122	0.5	4.6857
1.5	0,112	0.113	0.0013	5.122	0.5	5.0761

Based on Table 2, the resulting film thickness shows an increase with increasing concentration of impurities. Bismuth has an ionic radius of 1.32 Å while strontium and titanium have ionic radii of 1.17 Å and 0.75 Å, respectively [19]. This is because bismuth has an ionic radius that is closer to hat of strontium so the larger bismuth ionic radius will replace the strontium ionic radius. This also causes an increase in viscosity because the concentration of the solution is the large number of particles dissolved in each volume so the greater the concentration, the greater the friction that occurs between the particles [19]. The smallest film thickness was shown at a concentration of 0%, namely 3.9047 μm, while the largest thickness was shown at a concentration of 1.5%, namely 5.0761 μm.

3.2 Optical Properties of $SrTiO_3$

The optical properties were tested using a UV-Vis spectrophotometer and the values of reflectance, transmittance, and absorption could be known.

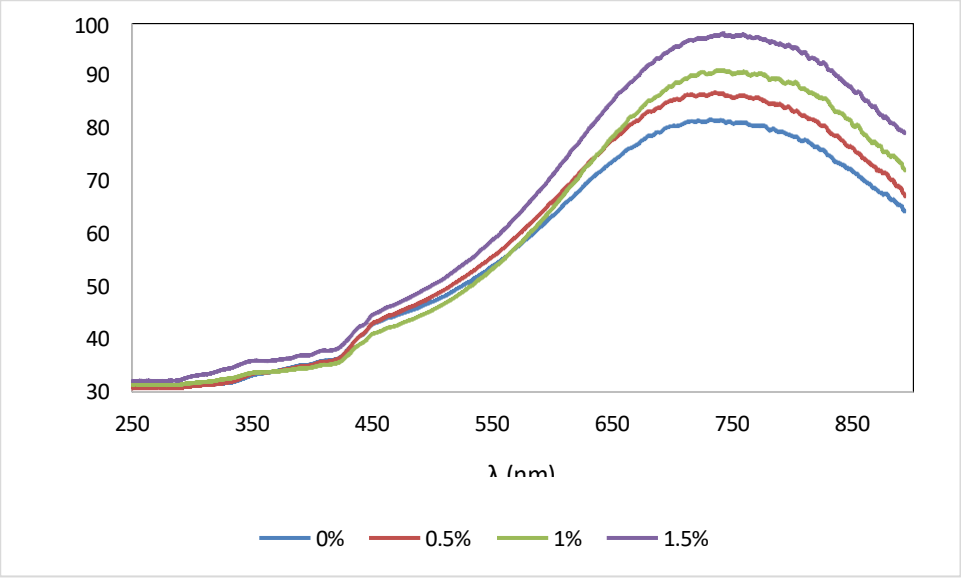

Figure 3. Relationship between λ (nm) and reflectance (%).

Figure 3 is the relationship between reflectance (%) and λ or wavelength (nm) and it can be seen that the intensity of the reflectance has increased significantly from 450 nm to 850 nm. The reflectance value increases as the concentration of impurities increases. In the opinion of [20], an increase in the reflectance value and an increase in the concentration of impurities will result in fewer photons being absorbed so that the resulting band gap energy gets smaller.

The energy gap in Figures 4 is determined using a tauc plot by drawing a straight line between the absorption coefficient or x-axis (hv) and the absorption coefficient for photons or y-axis $(ahv)^2$ so that band gap energy is obtained [21].

The band gap energy obtained from Figure 4 shows a decrease with increasing impurity which indicates that it is easier for electrons to move from the valence band to the conduction band. The decrease in band gap energy is due to the addition of impurities (bismuth) on the surface of the $SrTiO_3$ film. Silicon is considered p-type, so the thin film part is n-type. It belongs to the metal element and functions to change the properties of a material [21].

The band gap energy obtained from Figure 4 shows a decrease with increasing impurity which indicates that it is easier for electrons to move from the valence band to the conduction band. The decrease in band gap energy is due to the addition of impurities (bismuth) on the surface of the $SrTiO_3$ film. Silicon is considered p-type, so the thin film part is n-type and belongs to the metal element and functions to change the properties of a material [21].

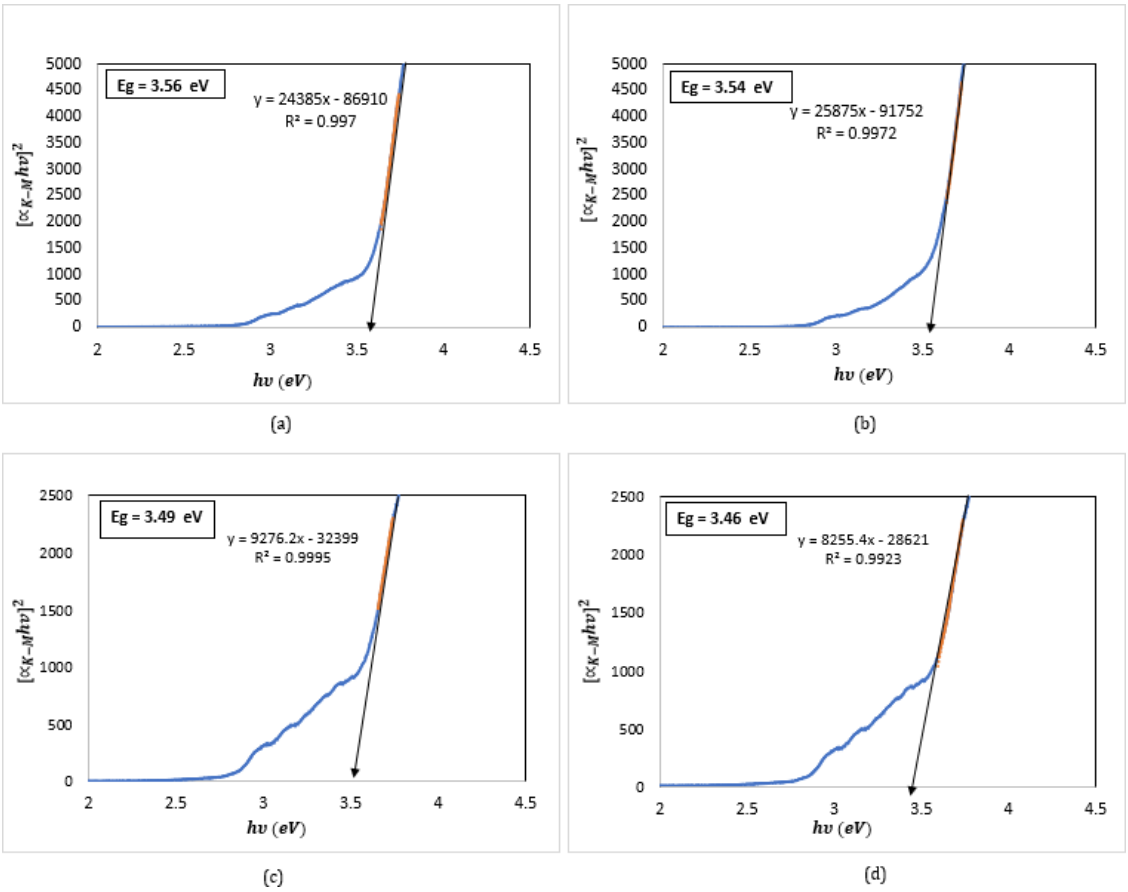

Figure 4. Graph of $SrTiO_3$ band gap energy (a) without impurities; (b) with 0.5% of $Bi(CH_3COO)_3$ impurity; (c) with 0.5% of $Bi(CH_3COO)_3$ impurity; (d) with 0.5% of $Bi(CH_3COO)_3$ impurity.

Table 3 Band gap energy of $SrTiO_3$ thin films with $Bi(CH_3COO)_3$ impurities

Impurity Variation		Band Gap Energy (eV)	Band Gap Energy Literature (eV)
		Direct Transition (n=2)	Direct Transition [8]
$SrTiO_3$+ 0%	$Bi(CH_3COO)_3$	3.56	3.75
$SrTiO_3$ + 0.5%	$Bi(CH_3COO)_3$	3.54	
$SrTiO_3$ + 1%	$Bi(CH_3COO)_3$	3.49	
$SrTiO_3$ + 1.5%	$Bi(CH_3COO)_3$	3.46	

Table 3 above represents the band gap energy values from the results of reflectance spectrum analysis using the Kubelka-Munk direct transition function equation (n=2). The energy in Table 3 can be seen decreasing with increasing impurities with the largest band gap energy occurring at 0% impurity, namely 3.57 eV, and the lowest band gap energy occurring at 1.5% impurity, namely 3.46 eV. The band gap energy in the literature is 3.75 eV.

3.3 Data Analysis with Cramer-Cohen

This study used XRD Bruker D8 ADVANCE to determine the lattice parameters and crystal structure of $SrTiO_3$ films. XRD characterization was carried out after the annealing stage and produced a relationship curve between the intensity and 2θ, the range of graphs displayed in the images and analyzed is 20o to 80o as shown in Figure 5. The data were analyzed using the Cramer- Cohen method and Excel software. The output is intensity data and 2θ.

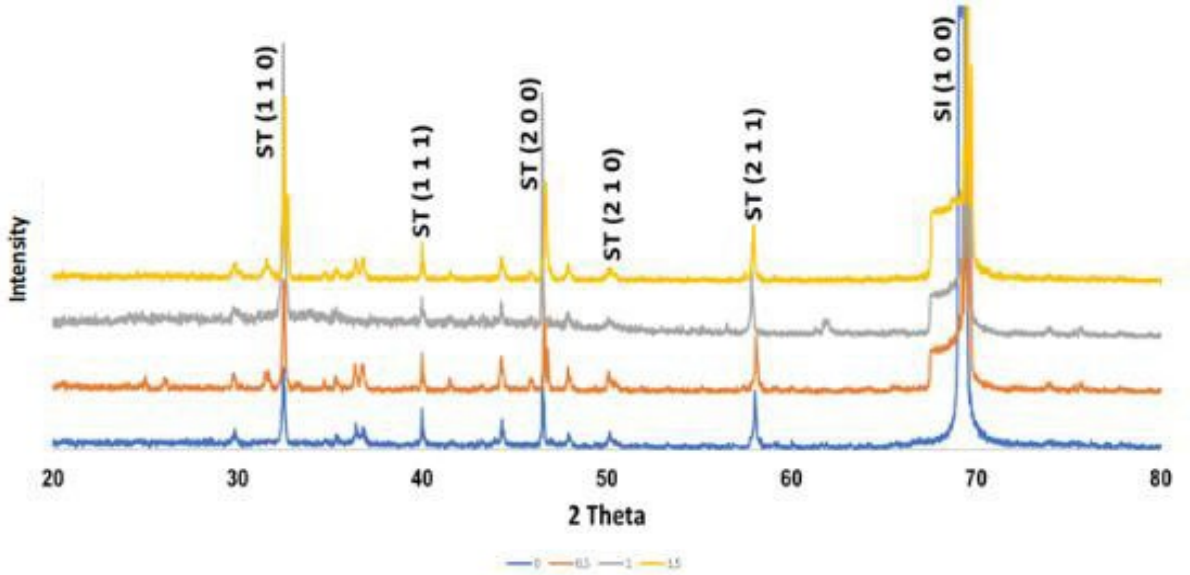

Figure 5. Relationship between 2θ and SrTiO3 intensity.

The graph Figure 5 shows the peaks distributed in the range of 20o to 80o which means that crystals form on the $SrTiO_3$ film. The diffraction peaks that are formed are then matched with data from the International Center for Diffraction Data (ICDD no. 35-0734) for $SrTiO_3$ materials so that the Miller index (hkl) can be known. The Miller index obtained was then analyzed using the Cramer- Cohen method so that the lattice parameters could be determined. The lattice parameters that have been obtained are then re-matched with ICDD no. 35-0734 so that the effect of adding $Bi(CH_3COO)_3$ impurities on $SrTiO_3$ thin films can be known.

Table 4 Lattice parameters of SrTiO3 thin films with Bi(CH3COO)3 impurities with a cubic structure using the Cramer-Cohen method

Impurity Variation	**Lattice parameters (Å) a = b = c**	**ICDD Literature (ICDD no. 35-0734) (Å) a = b = c**
$SrTiO_3$	3.835	3.905
$SrTiO_3$+ $Bi(CH_3COO)_3$ 0.5 %	3.837	
$SrTiO_3$+ $Bi(CH_3COO)_3$ 1 %	3.909	
$SrTiO_3$ + $Bi(CH_3COO)_3$ 1.5 %	3.913	

Based on Table 4, the results of the analysis using the Cramer-Cohen method show the lattice parameters a=b=c, so that the structure of the $SrTiO_3$ film is in the shape of a cube. The lattice parameter values for each impurity were 3.835 Å, 3.837 Å, 3.909 Å, 3.913 Å, and the literature lattice parameters were 3.905 Å. The lattice parameter values that are quite close between the

experiment and the literature are found in 1% impurities with an experimental value of 3.909 Å and a literature value of 3.905 Å. The difference is 0.004 Å. Lattice parameters increase with increasing impurity concentration. This is because the ionic radius of bismuth (1.32 Å) is larger than that of strontium (1.17 Å), so bismuth will replace strontium in thin films. Figure 6 shows that the doping bismuth has entered the strontium host [22]. This replacement causes the lattice parameter values to increase, and effects the XRD spectral curve at the preferred peak (2 1 1) shift to the left (Figure 7).

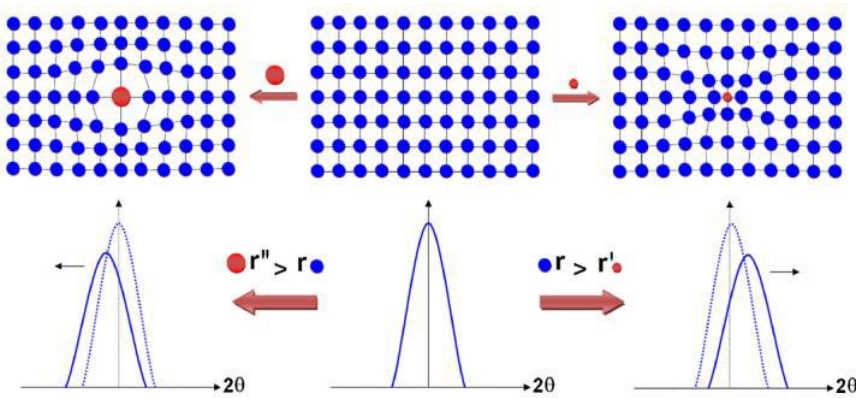

Figure 6. The relationship of the ionic radius of the doping to its host [22]

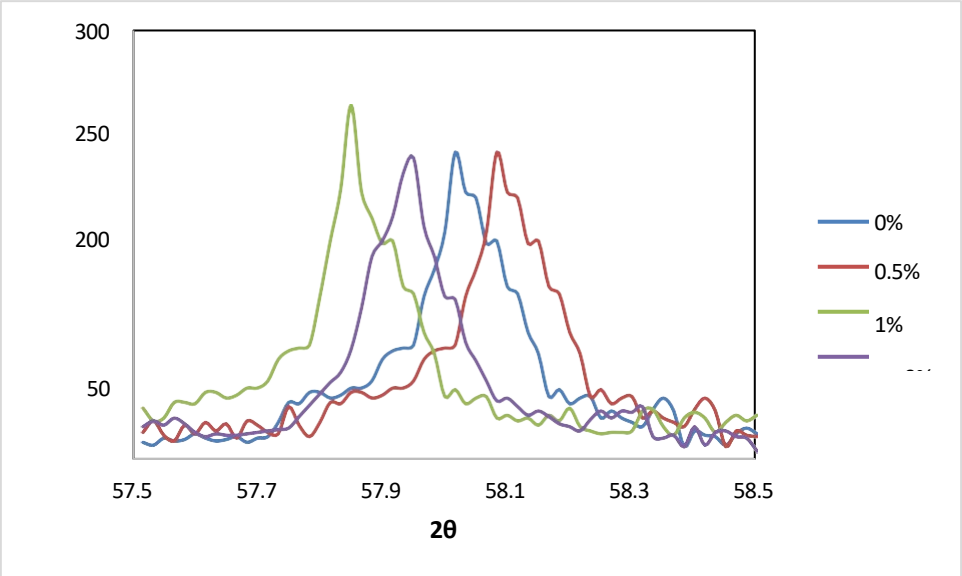

Figure 7. Relationship between 2θ and $SrTiO_3$ intensity in the XRD spectral curve at the preferred peak (2 1 1).

3.4 Analysis and Characterization Results of XRD using the MAUD Tool

Analysis of XRD data with the MAUD tool using the Rietveld method with 5 iterations produced a graph of the smoothed $SrTiO_3$ film diffraction pattern. Figures 8, 9, 10, and 11 are the results of XRD data analysis. The R_{exp} value and sigma value are one of the success factors for the MAUD tool as shown in Table 5.

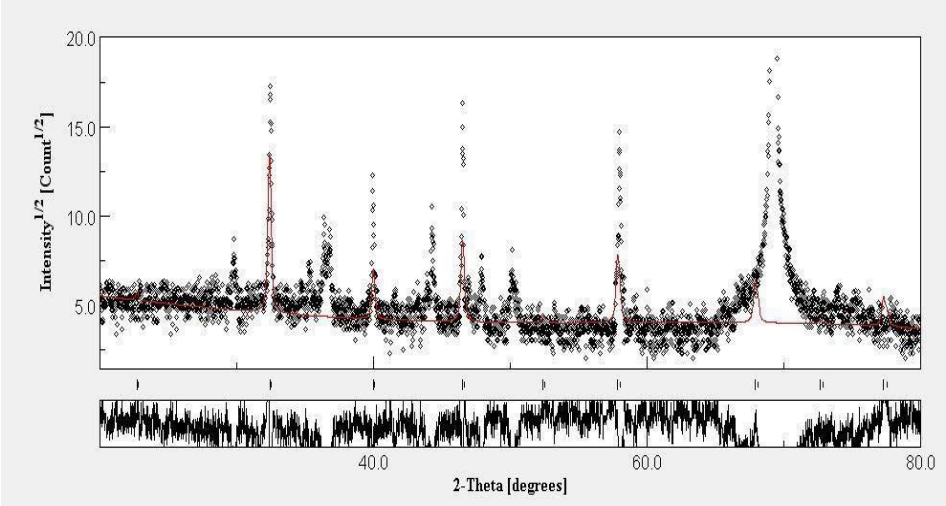

Figure 8. Graph of $SrTiO_3$ film diffraction pattern without impurities.

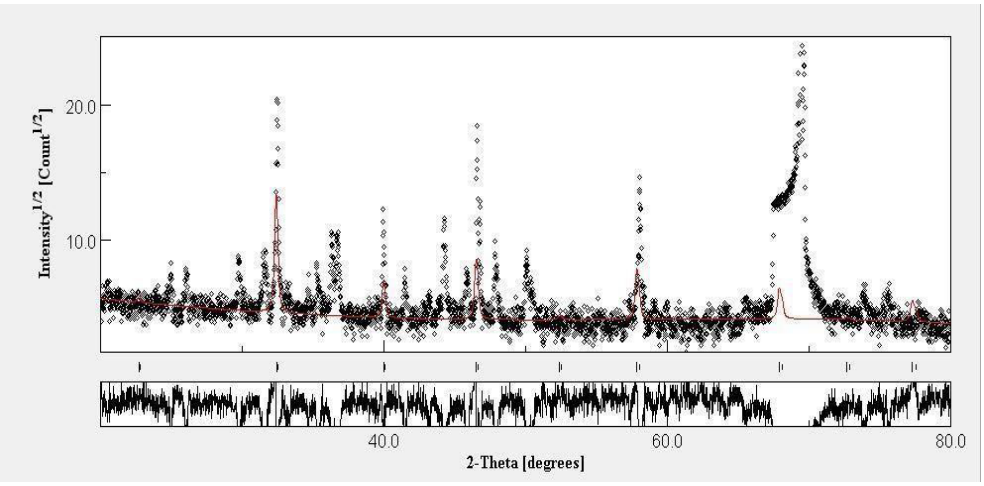

Figure 9. Graph of $SrTiO_3$ film diffraction pattern with 0.5% of $Bi(CH_3COO)_3$ impurity.

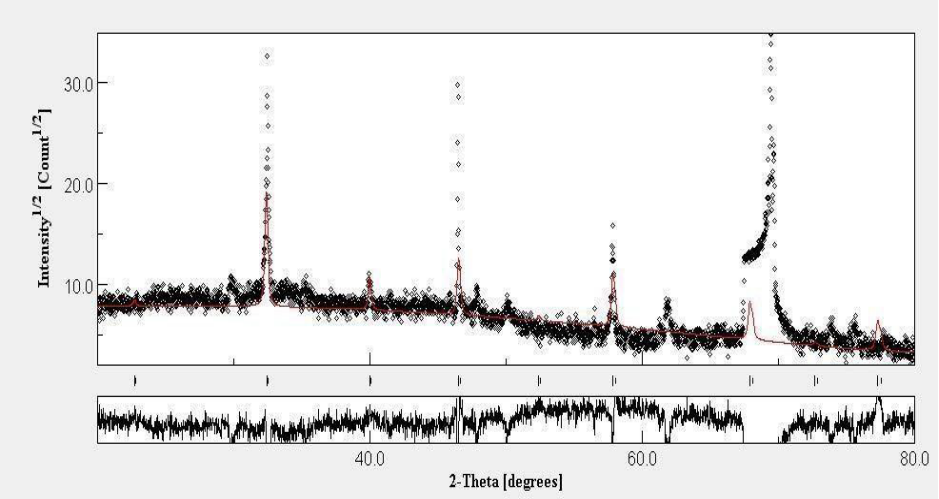

Figure 10. Graph of $SrTiO_3$ film diffraction pattern with 1% of $Bi(CH_3COO)_3$ impurity.

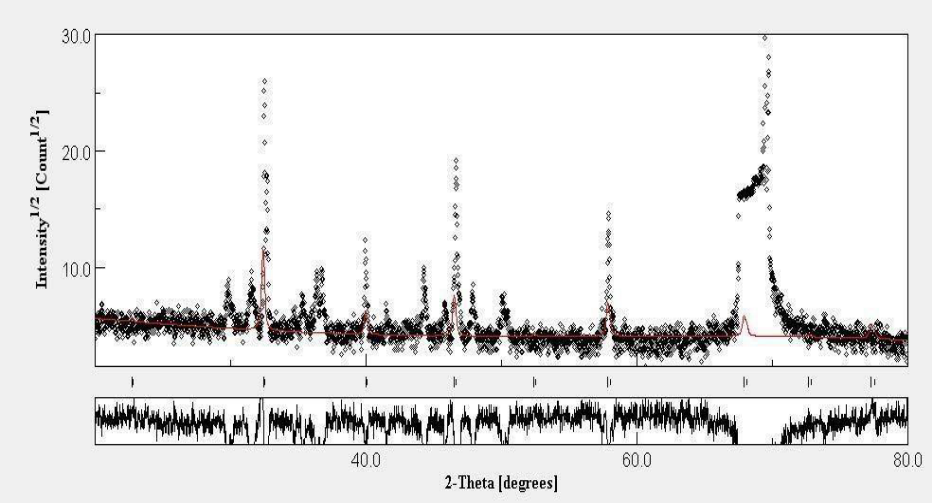

Figure 11. Graph of $SrTiO_3$ film diffraction pattern with 1.5% of $Bi(CH_3COO)_3$ impurity.

Table 5 Parameters of $SrTiO_3$ thin film lattice with $Bi(CH_3COO)_3$ impurity and cubic structure using the MAUD tools

Impurity Variation	Lattice Parameter Cramer-Cohen a = b = c	ICDD no. 35-0734 Literature a = b = c	Lattice Parameters MAUD a = b = c	R_{exp}	Sigma
$SrTiO_3$ + 0% $Bi(CH_3COO)_3$	3.835	3.905	3.846	16.425	3.845
$SrTiO_3$ + 0.5% $Bi(CH_3COO)_3$	3.837		3.848	17.072	3.260
$SrTiO_3$ + 1% $Bi(CH_3COO)_3$	3.909		3.925	13.760	3.330
$SrTiO_3$ + 1.5% $Bi(CH_3COO)_3$	3.913		3.961	16.773	3.711

Based on the lattice parameter data in Table 5, the lattice parameter values obtained with the MAUD tools are close enough to the ICDD no. 35-0734 data. The data above experienced a significant increase from 0.5% to 1% but the overall MAUD data have an increasing value like the Cramer-Cohen method. Lattice parameters in MAUD processing have values that are almost the same as in the literature when the impurity concentration is 1%. MAUD and literature lattice parameters have a difference of 0.020 Å with R_{exp} and sigma 13.760 and 3.330 respectively. If the R_{exp} value is less than 20 and the sigma value is less than 4, but the lattice parameter values are close to, it can be stated that the MAUD analysis was successful. So that the structure formed is a cube. Figure 12 shows the shape of the SrTiO3 structure for each impurity concentration.

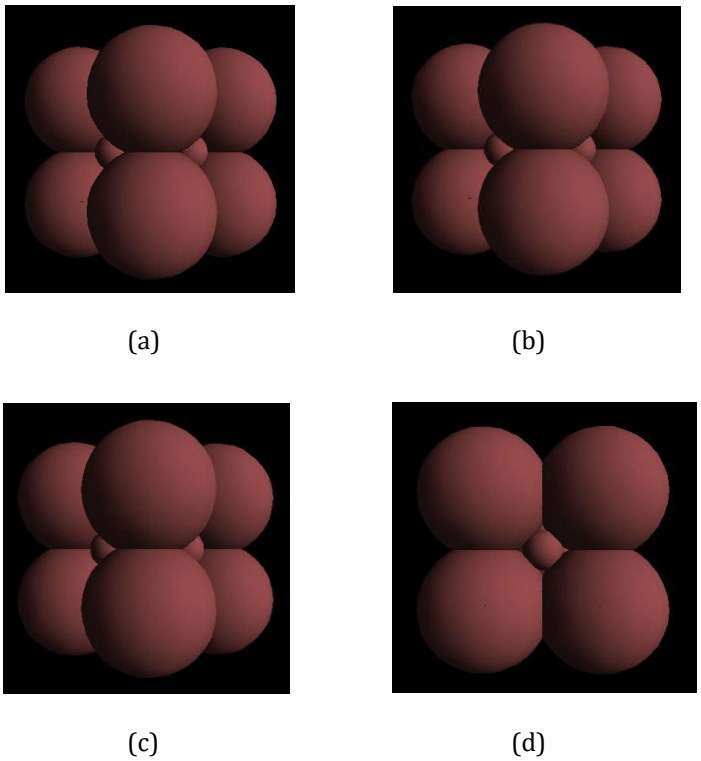

(a) (b)

(c) (d)

Figure 12. $SrTiO_3$ film structure with impurities
(a) 0% $Bi(CH_3COO)_3$ (b) 0.5% $Bi(CH_3COO)_3$
(c) 1% $Bi(CH_3COO)_3$ (d) 1.5% $Bi(CH_3COO)_3$

4. CONCLUSION

$SrTiO_3$ thin films have been successfully created using the CSD method and spin coating technique with variations in $Bi(CH_3COO)_3$ impurities of 0%, 0.5%, 1%, and 1.5%. The film thickness was determined by the volumetric method, resulting in values of 3.9 μm, 4.3 μm, 4.7 μm and 5.1 μm. The optical properties test on the $SrTiO_3$ film showed that the addition of impurity concentrations would decrease the band gap energy. In this case, the impurity serves to reduce the band gap energy, making it easier for electrons to be excited from the valence band to the conduction band. From the analysis of optical properties with the Kubelka-Munk function for the direct transition, a band gap of 3.46 - 3.56 eV is obtained. On the other hand, from the crystal properties test, it was found that the addition of impurities would increase the lattice parameters. This is because the ionic radius of the impurities of Bi^{3+} is larger than the ionic radius of Sr^{2+}, so Bi^{3+} replaces Sr^{2+} in $SrTiO_3$. Analysis of the XRD results was carried out using the Cramer-Cohen method and obtained lattice parameters (a=b=c) of Strontium Titanate ($SrTiO_3$) doped with Bismuth Acetate ($Bi(CH_3COO)_3$) with various concentrations of 0%; 0.5%; 1%; and 1.5% are 3.835 Å, 3.837 Å, 3.909 Å, 3.913 Å respectively with a cubic crystal structure.

REFERENCES

[1] Istiqomah M, Jamaluddin A, Iriani Y. 2014. Pembuatan material feroelektrik barium titanat ($BaTiO_3$) menggunakan metode solid state reaction. Jurnal Fisika Indonesia. 18(53): 59- 61.

[2] Iskandar J, Jenie RP, Siregar UJ, Yuliarto B, Irzaman. 2020. Application of thin film barium strontium titanate (BST) in a microcontroller-based tool to measure oxygen saturation in blood. Ferroelectrics. 554(1): 134-143.

[3] Rofiko H, Iriani Y, dan Suryana R. 2017. Pengaruh suhu sintering pada pembuatan Stronsium titanat (SrTiO3) terhadap konstanta dielektrik menggunakan metode Co-Precipitation. Indonesian Journal of Applied Physics. 7(1): 28-35.

[4] Zhang Y, Zhong L, Duan D. 2015. Single-step hydrothermal synthesis of strontium titanate nanoparticles from crystalline anatase titanium dioxide. Ceramics International. 41: 13516-13524.

[5] Putri YE, Najela R, Andriani N, Wellia DV. 2021. SrTiO3 Nanokubus: Sintesis, kontrol, morfologi dan sifat termoelektrik. Akta Kimindo. 6(1): 83-126.

[6] Habibie K, Syifa NA, Bahtiar A. 2019. Pengaruh penyisipan ion bromida terhadapsifat optic dan struktur kristal lapisan tipis perovskite halide campuran MAPbBrxI3-x. Jurnal Material dan Energi Indonesia. 9(2): 71-78.

[7] Liu X, Sohiberg K. 2014. Theoretical calculations on layered perovskites: Implications for photocatalysis. Complex Metals. 1(1): 103-121.

[8] Benthem V, Elsasser K, French RH. 2011. Bulk electronic structure of SrTiO3: experiment and theory. J of Applied Physics. 90(12): 6156-6164.

[9] Bothwell JM, Krabbe SW, Mohan RS. 2011. Applications of bismuth (III) compounds in organic synthesis. Chemical Society Reviews. 40(9): 4649- 4707.

[10] Duan X, Yang J, Zhu W, Fan X, Xiao C. 2007. Structure and electrical properties of bismuth thin films prepared by flash evaporation method. Material Letters. 61(22): 4341-4343.

[11] Champs E, Rodil SE, Salas JA, Estrada HV. 2012. A detailed study of the synthesis of bismuth thin films by PVD methods and their structural characterization. Material Research Society.

[12] Pereira JR, Ortiz SAR, Ospina R. 2020. Bismuth acetate by XPS. Surface Science Spectra. 27(2): 1-7.

[13] Rahmawaty V, Sumaryada T, Irzaman. 2019. Optical properties and microstructurerietveld analysis of CeO2-doped SrTiO3 thin film. AIP Conference Proceedings. 2202(1):1-9.

[14] Muhlis, Fathoni I, Iswarin SJ, Triandi R, Masruroh. 2013. Studi penumbuhan lapisan tipis PZT dengan metode spin coating. Brawijaya Physics Student Journal. 1(1): 53-56.

[15] Irzaman, Rahmawaty V, Palupi EK, Patonah N, Sumaryada T, Siskandar R, Alatas H, Iqbal M, Yuliarto B, Fahmi MZ, Rusydi F, Nugroho WS. 2021. The effect of photoconductive mole fraction based on thin film BaxSr1-xTiO3 (x=0.000; 0.125; 0.250; 0.375; 0.500) on electrical properties and diffusivity coefficient. Biointerface Research in Applied Chemistry. 11(6): 14956-14963.

[16] Irzaman, Siskandar R, Jenie RP, Syafutra H, Iqbal M, Yuliarto B, Fahmi MZ, Ferdiansjah, Khairurrijal. 2022. Ferroelectric sensor BaxSr1-xTiO3 integrated with android smarthphone for controlling and monitoring smart street lighting. Journal of King Saud University. 6(34): 102180. doi: 10.1016/j.jksus.2022.102180.

[17] Irzaman, Siskandar R, Yuliarto B, Fahmi MZ, Ferdiansjah. 2019. Application of Ba0.5Sr0.5TiO3(BST) film doped with 0%, 2%, 4%, and 6% concentrations of RuO2 as an Arduino nano-based bad breath sensor. Chemosensors. 8(3): 1-11.

[18] Putri D, Darvina Y, Yulkifli, Ramli. 2019. Pengaruh komposisi terhadap ukuran butir lapisan nanokomposit CoFe2O4/PVDF dengan metode spin coating. Pillar of Physics. 12: 84-90.

[19] Irzaman, Zuhri M, Novitri, Irmansyah, Setiawan AA, Alatas H. 2019. Surface morphology properties doped RuO2 (0, 2, 4, 6%) of thin film LiNbO3. Journal of Physcis: Conference Series. 755(1): 7-11. doi: 10.1088/1742-6596/1282/1/012040.

[20] Irzaman, Nuraisah A, Aminullah, Hamam KA, Alatas H. 2018. Optical properties and crystal structure of lithium doped Ba0.55Sr0.45TiO3 (BLST) thin films. Ferroelectrics Letters Section. 45(1): 14-21. doi: 10.1080/07315171.2018.1499361.

[21] Indriani D, Fahyuan HD, Ngatijo. 2018. Uji UV-Vis lapisan TiO2/N2 untuk menentukan band gap energy. Journal of Physics. 3(2): 6-10.

[22] Khorrami H, Zak AK, Kompany A, Yousefi R. 2012. Optical and structural properties of X-doped (X = Mn, Mg, dan Zn) PZT nanoparticles by Kramers-Kronig and size strain plot methods. Ceramics International. 38(7): 5683-5690. doi: 10.1016/j.ceramint.2012.04.012.